Predicting Chronic Myocardial Ischemia Using CCTA-Based Radiomics Machine Learning Nomogram

Zhen-Yu Shu, MD,[a] Si-Jia Cui, MD,[b] Yue-Qiao Zhang, MD,[c] Yu-Yun Xu, MD,[a] Shng-Che Hung, MD,[d,e] Li-Ping Fu, MD,[f] Pei-Pei Pang, MD,[g] Xiang-Yang Gong, MD, PhD,[a,h] and Qin-Yang Jin, MD[a]

[a] Department of Radiology, Zhejiang Provincial People's Hospital, Affiliated People's Hospital of Hangzhou Medical College, Hangzhou, Zhejiang, China
[b] Second Clinical College, Zhejiang Chinese Medical University, Hangzhou, China
[c] Department of Radiology, Shao-Yifu Hospital Affiliated to Zhejiang University, Hangzhou, China
[d] Division of Neuroradiology, Department of Radiology, University of North Carolina School of Medicine, Chapel Hill, NC
[e] Biomedical Research Imaging Center, University of North Carolina at Chapel Hill, Chapel Hill, NC
[f] Department of Nuclear Medicine, Zhejiang Provincial People's Hospital, Affiliated People's Hospital of Hangzhou Medical College, Hangzhou, China
[g] GE Healthcare China, Shanghai, China
[h] Institute of Artificial Intelligence and Remote Imaging, Hangzhou Medical College, Hangzhou, China

Received Feb 14, 2020; accepted May 5, 2020
doi:10.1007/s12350-020-02204-2

Background. **Coronary computed tomography angiography (CCTA) is a well-established non-invasive diagnostic test for the assessment of coronary artery diseases (CAD). CCTA not only provides information on luminal stenosis but also permits non-invasive assessment and quantitative measurement of stenosis based on radiomics.**

Purpose. **This study is aimed to develop and validate a CT-based radiomics machine learning for predicting chronic myocardial ischemia (MIS).**

Methods. **CCTA and SPECT-myocardial perfusion imaging (MPI) of 154 patients with CAD were retrospectively analyzed and 94 patients were diagnosed with MIS. The patients were randomly divided into two sets: training (n = 107) and test (n = 47). Features were extracted for each CCTA cross-sectional image to identify myocardial segments. Multivariate logistic regression was used to establish a radiomics signature after feature dimension reduction. Finally, the radiomics nomogram was built based on a predictive model of MIS which in turn was constructed by machine learning combined with the clinically related factors. We then validated the model using data from 49 CAD patients and included 18 MIS patients from another medical center. The receiver operating characteristic curve evaluated the diagnostic**

Electronic supplementary material The online version of this article (https://doi.org/10.1007/s12350-020-02204-2) contains supplementary material, which is available to authorized users.

The authors of this article have provided a PowerPoint file, available for download at SpringerLink, which summarizes the contents of the paper and is free for re-use at meetings and presentations. Search for the article DOI on SpringerLink.com.

Zhen-Yu Shu and Si-Jia Cui contributed equally to this work.

Reprint requests: Xiang-Yang Gong, MD, PhD, Department of Radiology, Zhejiang Provincial People's Hospital, Affiliated People's Hospital of Hangzhou Medical College, No. 158 Shangtang Road, Hangzhou, Zhejiang, China; *cjr.gxy@hotmail.com*

1071-3581/$34.00

accuracy of the nomogram based on the training set and was validated by the test and validation set. Decision curve analysis (DCA) was used to validate the clinical practicability of the nomogram.

Results. **The accuracy of the nomogram for the prediction of MIS in the training, test and validation sets was 0.839, 0.832, and 0.816, respectively. The diagnosis accuracy of the nomogram, signature, and vascular stenosis were 0.824, 0.736 and 0.708, respectively. A significant difference in the number of patients with MIS between the high and low-risk groups was identified based on the nomogram ($P < .05$). The DCA curve demonstrated that the nomogram was clinically feasible.**

Conclusion. **The radiomics nomogram constructed based on the image of CCTA act as a non-invasive tool for predicting MIS that helps to identify high-risk patients with coronary artery disease. (J Nucl Cardiol 2022;29:262–74.)**

Key Words: Radiomics • coronary CT angiography • myocardial ischemia • nomogram • machine learning

See related editorial, pp. 275–277

INTRODUCTION

Coronary artery disease (CAD) is the leading cause of cardiovascular mortality and morbidity across the globe.[1] Majority of the CAD patients present with clinically stable ischemic heart disease. The implementation of revascularization in these patients mainly refers to the degree of myocardial ischemia (MIS) and not the severity of CAD.[2] The presence of moderate-to-severe ischemia remains the mandatory criterion for percutaneous coronary intervention in stable CAD.[3] Therefore, the assessment of MIS in these patients has a direct impact on the treatment of CAD.

Coronary computed tomography angiography (CCTA) provides information on coronary artery anatomy and stenosis. Furthermore, it helps to detect and evaluate coronary artery stenosis and atherosclerotic plaque.[4] Hence, CCTA is commonly used to assess patients suspected of CAD and patients with low or moderate levels of risk.[5] However, coronary artery stenosis and blood flow changes in the myocardium are not related. Therefore, the hemodynamic significance in assessing coronary artery lesions by CCTA alone remains uncertain.[6,7] This limitation is evident in patients at high risk of CAD.[8] Irrespective of the fact that myocardial perfusion imaging using dual-source CT directly visualizes myocardial iodine content and identifies MIS [9,10] it is difficult to distinguish sclerosis artifact of the X-ray beam and perfusion defect of MIS as they are similar and leads to a false-positive result.[11] Conventional CCTA images show limited contrast and hence the evaluation of MIS by visual changes on myocardial tissue density becomes deficient. Thus, it is important to combine other functional tests to assess MIS.[12]

Radiomics is a new quantitative imaging technology that has been widely used in medical research due to its cost-effectiveness and non-invasive nature.[13,14] Radiomics refers to the extraction of quantitative features from medical images to develop predictive or prognostic models for disease treatment. Radiomics analysis can be applied for preliminary diagnosis [15] including myocardial infarction,[16] cardiomyopathy,[17,18] myocarditis [19] and arrhythmia.[20] However, to the best of our knowledge, there no studies that quantitatively assess MIS using radiomics. Also, we do not know whether radiomics can differentiate between an MIS and normal myocardium; however, we hypothesize that the radiomics analysis of CCTA images can distinguish MIS from normal myocardium, and the potential benefit of this hypothesis is that CCTA is used as a one-stop non-invasive examination to simultaneously examine coronary artery anatomy and assess hemodynamic information.

Furthermore, by correlating radiomics with clinical data, we can establish disease prediction models.[21,22] Hence, the study is aimed to develop and validate a radiomics nomogram for predicting MIS using conventional CCTA.

MATERIALS AND METHODS

Patients Information

We obtained study approval from the Ethics Committee of ZJP hospital (Hangzhou, Zhejiang Province, China) with a waiver for obtaining informed consent from the patients. We retrospectively analyzed data of patients who underwent both CCTA and myocardial perfusion imaging (MPI) at ZJP hospital from May 2017 to March 2020. The period between the two examinations was not more than 7 days. Patient inclusion criteria were as follows: (1) patients without myocardial infarction within the last three months, (2) patients with typical or atypical symptoms of angina pectoris patients persisting for > 2 months, (3) patients with abnormalities in ECG or treadmill exercise test, (4) good quality images of CCTA includes no obvious motion artifact, no metal stent artifact and the use of good contrast agent to improve the visibility of the blood vessel (5) patients with no other heart

disease. Patient exclusion criteria were as follows: (1) patients with a history of coronary artery bypass or stent implantation, (2) patients with rapid heart rate (heart rate greater than 85 beats per minute or arrhythmia, (3) patients with liver or kidney dysfunction. In this study, we enrolled 154 patients following the guidelines of the American Heart Association (AHA) and 93 patients were diagnosed with MIS using single-photon emission computed tomography (SPECT)-MPI, a gold standard for the evaluation of MIS.[4] Details of the MPI are provided in the Supplementary Material. Also, we divided the patients into two sets—training and test—in the ratio 7:3. The training set consisted of patients enrolled between May 2017 and April 2019, whereas the test set composed of patients enrolled between May 2019 and March 2020. The training set was used to examine the robustness of radiomic features and to construct a predictive model. The test set was used to verify the reliability of the predictive model. We also collected CCTA data from 49 patients between August 2018 and March 2020 from SYF hospital (Hangzhou, Zhejiang Province, China) for external validation. The flowchart of the recruitment process and research design is shown in Figure 1.

CCTA Acquisition

All patients underwent a prospective electrocardiogram (ECG)-gated cardiac CT angiography by two different vendors with ≥ 64 detector rows (Aquilion One, Toshiba Medical Systems, Otawara, Japan; Somatom Flash/Force, Siemens Healthineers, Forchheim, Germany). Detailed information on scanning parameters and CCTA are provided in the Supplementary Material. After scanning, the best time phase of the display of the coronary artery of imaging was chosen and transferred into the workstation for reconstructing the coronary artery with volume rendering, curved planar reconstruction, and multi-planar reconstruction. The AHA recommends a 15-segment coronary artery method,[23] which was followed by two experienced radiologists to evaluate vascular stenosis. When

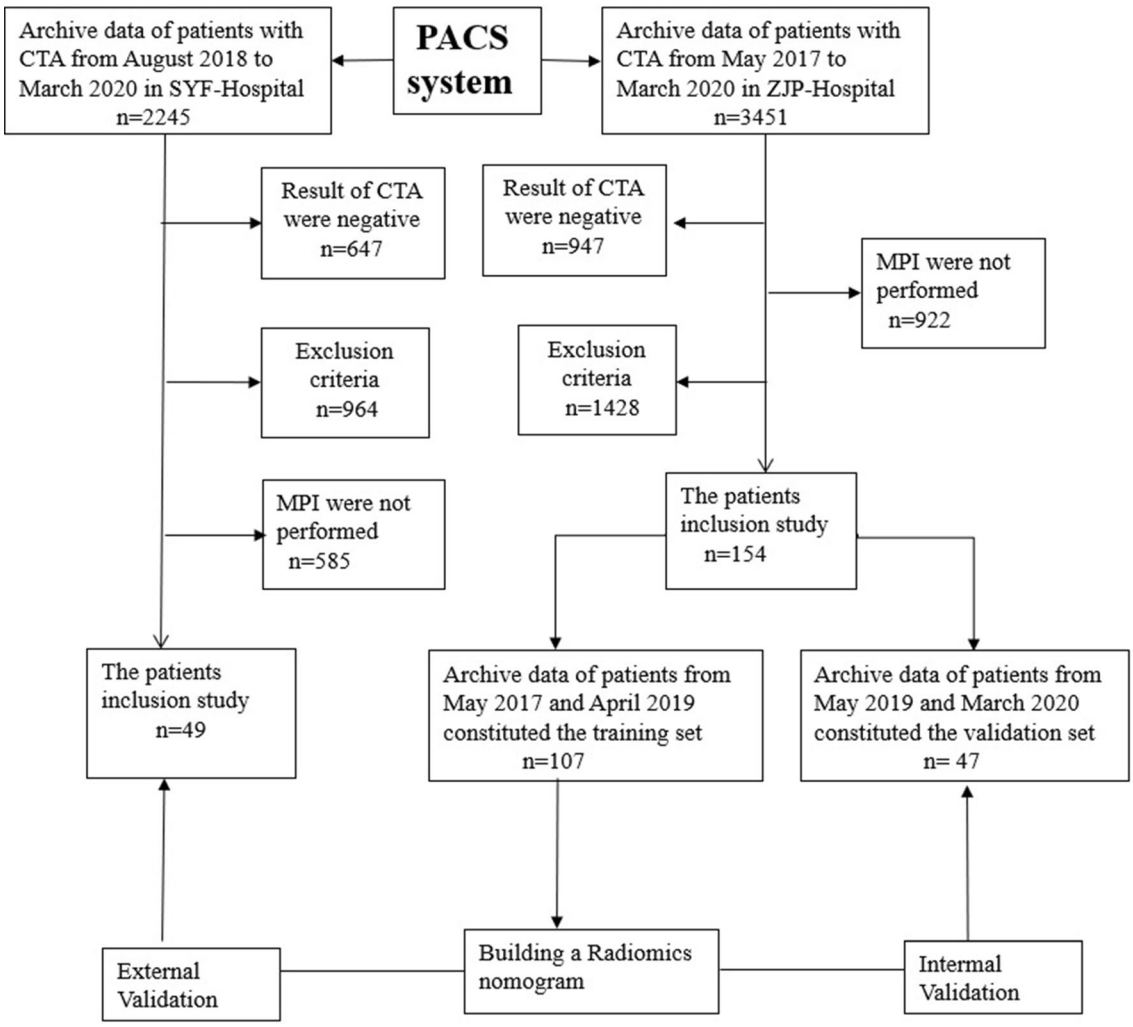

Figure 1. Flowchart of patient recruitment and study design.

there was a difference in opinion, they concluded after discussing it in detail.

A modified Gensini scoring system [24] was used to include heavier stenosis lesions in each vascular segment. The degree of coronary artery stenosis in the lesion was scored as follows: 0 point—no abnormality; 1 point—stenosis between 1 and 49%; 2 points—stenosis from 50 to 74%; 3 point—stenosis from 75 to 99%; 4 points—occlusion of the artery (100%). The sum of the scores of each segment is the total score of the patient. According to the improved Gensini scoring system, coronary artery stenosis is graded as mild (1 to 14 point) and severe stenosis (> 14 points).

CCTA Image Features Extraction

The CCTA images of the arterial phase of each patient were imported into the CQK analysis platform (CT Coronary Artery Quantitative Analysis Kit, version 1.2, GE Healthcare) in DICOM format for the automatic segmentation of myocardial. A three-dimensional (3D) image of myocardium was obtained. To reduce error of automatic image segmentation, the 3D-image was manually modified by two experienced radiologists who were blinded to the clinical information. The manual correction steps included: (1) removing non-myocardial tissue; (2) removing myocardial fibrous filaments; (3) correcting segmentation errors in myocardial tissue, and finally image preprocessing included resampling the image to $1 \times 1 \times 1$ mm^3 voxel size, and standardizing the gray level to 1 to 32 scales[25] before feature extraction. The software package for image analysis is attached to the CQK platform to extract radiomics features. The 3D myocardial images included Histogram, Haralick, FormFactor, gray level co-occurrence matrix (GLCM), Run-length matrix (RLM) and gray level size zone matrix features. These features characterize cancer heterogeneity and potentially reflect changes in image structure.[26] Besides, we used the features that are more robust after manual correction by two radiologists[27] to ensure reproducibility and repeatability of radiomics features. Spearman's rank correlation test was used to calculate the correlation coefficient between feature set A (from Radiologist A) and feature set B (from Radiologist B). Features with correlation coefficient > 0.8 were regarded as robust according to a rule of thumb.[28]

Radiomics Signature Establishment

The maximum relevance minimum redundancy (mRMR) algorithm was used to extract the robust features in the training set.[29] The maximum relevance selection aimed to select features that had a maximal correlation to the actual MIS. At the same time, the minimum redundancy selection ensured that the selected features had minimal redundancy among each other. The mRMR method was used to obtain optimal features set with high correlation and low redundancy.[30] Then, the typical gradient boosting decision tree algorithm was used to reduce the dimension and construct the radiomics signature using multivariate logistic regression. The signature model of the training set that reflects MIS probability was used to calculate the radiomics score (rad-score) that discriminates the capacity of signature models in separating patients with MIS and non-MIS. The formula of the model in the training set was also used to calculate the score of the test set. Finally, the accuracy of the radiomics signature in the training and test set was calculated using the area under the curve (AUC) of the receiver operating characteristic (ROC) curve. Furthermore, we verified the clinical efficacy of the rad-score by performing a stratified analysis of rad-score in patients with vascular stenosis. Detailed information about dimensionality reduction and radiomics signature is provided in the Supplementary Material.

Construction and Evaluation of Radiomics Nomogram

Multivariable logistic regression analysis was performed to select independent predictors of MIS for each potential predictive variable that the clinical factors (gender, age, hypertension, diabetes, hyperlipidemia, smoking, alcohol intake, the grade of vascular stenosis and radiomics signature) in the training group. The co-linearity of each variable was diagnosed using the variance inflation factor (VIF)[22] and the variable VIF > 10 indicates severe multicollinearity.[31] Machine learning was applied to develop a predictive model for the MIS based on independent predictors, and a radiomics nomogram was constructed. In this study, the machine learning model was evaluated using tenfold cross-validation. 10% data was used to test the model and the other 90% to create the model. Different test and training set data were used for every tenfold cross-validation and the average classification accuracy calculated based on ten times tenfold cross-validation. Also, several machine learning methods including support vector machine (SVM), the K-nearest-neighbors (KNN) and Random Forest were used to compare and select the best stable classifier using relative standard deviation (RSD) and a bootstrap approach. It should be noted that higher stability in the case of classifiers corresponds to lower RSD values.[32] The calibration curve was used to evaluate the calibration performance and the Hosmer-Lemeshow test was used to analyze the fitness. The nomogram's diagnostic accuracy was evaluated using the ROC curve. Based on the nomogram the risk score of MIS was calculated for each patient. All patients were divided into high-risk groups and low-risk groups based on the cut-off value of the ROC curve. Based on the actual MIS patients in different risk groups the clinical effect of the nomogram was determined. The net benefit of the nomogram in training and test sets were evaluated using the decline curve analysis (DCA).[33,34] The definitions of relevant clinical factors and RSD are provided in the Supplementary Material.

Statistical Analysis

The statistical analyses were performed using SPSS software 17.0 (IBM, Armonk, NY), GraphPad (San Diego, CA), and R software (version 3.4.1; http://www.Rproject.org). The normality of distribution was evaluated using the Kolmogorov–Smirnov test. A Chi-squared test was used for categorical data. To determine whether the features were

significantly different between groups student's t-test was used for normally distributed features. However, the Mann-Whitney test was used otherwise. The ''rms'' package of R software was used to construct the nomogram and plot the calibration. Statistical significance was set at $P < .05$.

RESULTS

Comparison of Patients' Clinical Data

There were no significant differences in gender, age, hypertension, hyperlipidemia, diabetes, smoking and vascular stenosis between the training, test, and validation sets (Table 1). However, between MIS and non-MIS in the three set, there existed significant differences in vascular stenosis and rad-score (0.8994 ± 0.9148 vs − 0.1549 ± 1.293, 0.9931 ± 1.2369 vs. 0.4626 ± 0.8025, 0.8363 ± 0.8039 vs 0.1049 ± 0.7964, $P < .05$). The other factors showed no statistical differences (Table 2).

Radiomics Signature Development and Accuracy

Figure 2 shows the radiomics workflow. A total of 378 texture features were extracted. Of these, 198 radiomic features retained robustness and reproducibility. Finally, eight optimal features were obtained by dimensionality reduction. Details on dimensionality reduction are provided in the Supplemental Material. These eight features were used to construct the radiomics signature using multivariable logistic regression. The AUC, specificity, and sensitivity of the signature in the training set were 0.746%, 73.1%, and 68.1%, respectively, while in the test set 0.727%, 79.3%, and 71.1%, respectively. There was a significant difference in the rad-score between the non-MIS and MIS in the mild vascular stenosis subgroup, and the same results were found in the severe vascular stenosis subgroup (as shown in Figures 3 and 4).

Development Radiomics Nomogram

The multiple logistic regression analysis showed that vascular stenosis and rad-score were independent predictors of MIS. The variance inflation factor (VIF) values of vascular stenosis and rad-score were 1.003 and 1.024 respectively. This indicated that no serious co-linearity existed between these factors (Table 3). Also, we evaluated the RSD and accuracy for SVM, KNN, and Random Forest algorithms. The RSD values were 2.688, 3.468, and 5.941 for SVM, KNN, and Random Forest algorithms, respectively. The average AUC values were 0.838, 0.832 and 0.805 for SVM, KNN, and Random Forest algorithms, respectively (Table S3). Accordingly, the SVM was used to build the prediction models and construct a nomogram model. The calibration curves demonstrated good consistency between the predicted and the actual MIS probability for the radiomics nomogram in both training and test sets (Figure 5).

Table 1. Clinical characteristics of patients in the primary and internal validation cohorts

Variables		Training set (n=107) N (%)	Test set (n = 47) N (%)	Verification (n=49) N (%)	*P* value
Gender	Male	75 (70.1)	29 (61.7)	29 (59.2)	.302
	Female	32 (29.9)	18 (38.3)	20 (40.8)	
Age	Year	60.5 + 14.9	60.7 + 13.4	64.1 + 11.5	.342
Hypertension	No	58 (54.2)	20 (42.6)	24 (49)	.407
	Yes	49 (45.8)	27 (57.4)	25 (51)	
Hyperlipidemia	No	84 (78.5)	34 (72.3)	36 (73.5)	.648
	Yes	23 (21.5)	13 (27.7)	13 (26.5)	
Diabetes	No	88 (82.2)	34 (72.3)	35 (71.4)	.213
	Yes	19 (17.8)	13 (27.7)	14 (28.6)	
Alcohol intake in past 5 years	No	83 (77.6)	32 (68.1)	34 (69.4)	.365
	Yes	24 (22.4)	15 (31.9)	15 (30.6)	
Smoking in past 5 years	No	74 (69.2)	32 (68.1)	38 (77.6)	.503
	Yes	33 (30.8)	15 (31.9)	11 (22.4)	
Vascular stenosis	Mild	49 (45.8)	22 (46.8)	24 (49)	.935
	Severe	58 (54.2)	25 (53.2)	25 (51)	

Table 2. Clinical characteristics of the training and validation sets of myocardial ischemia patients

		Training set (n = 107)			Test set (n = 47)			Verification (n = 49)		
		MIS (n = 65)	No MIS (n = 42)		MIS (n = 28)	No MIS (n = 19)		MIS (n = 18)	No MIS (n = 31)	
Variable		**n (%)**	**n (%)**	***P* value**	**n (%)**	**n (%)**	***P* value**	**n (%)**	**n (%)**	***P* value**
Gender	Male	49 (75.4)	26 (61.9)	.137	17 (60.7)	12 (63.2)	.866	11 (61.1)	18 (58.1)	.834
	Female	16 (24.6)	16 (38.1)		11 (39.3)	7 (36.8)		7 (38.9)	13 (41.9)	
Age	62.5 ± 15.3		59.3 ± 14.5	.283	61.1 ± 14.3	60.2 ± 12.4	.825	65.7 ± 10.7	63.2 ± 12.1	.476
Hypertension	No	33 (50.8)	25 (59.5)	.375	14 (50)	6 (31.6)	.21	11 (61.1)	13 (41.9)	.196
	Yes	32 (49.2)	17 (40.5)		14 (50)	13 (68.4)		7 (38.9)	18 (58.1)	
Hyperlipidemia	No	50 (76.9)	34 (81)	.62	18 (64.3)	16 (84.2)	.134	13 (72.2)	23 (74.2)	.88
	Yes	15 (23.1)	8 (19)		10 (35.7)	3 (15.8)		5 (27.8)	8 (25.8)	
Diabetes	No	53 (81.5)	35 (83.3)	.812	23 (82.1)	11 (57.9)	.068	10 (55.6)	25 (80.6)	.061
	Yes	12 (18.5)	7 (16.7)		5 (17.9)	8 (42.1)		8 (44.4)	6 (19.4)	
Alcohol intake in past 5 years	No	48 (73.8)	35 (83.3)	.251	21 (75)	11 (57.9)	.217	12 (66.7)	22 (71)	.753
	Yes	17 (26.2)	7 (16.7)		7 (25)	8 (42.1)		6 (33.3)	9 (29)	
Smoking in past 5 years	No	45 (69.2)	29 (69)	.984	20 (71.4)	12 (63.2)	.551	13 (72.2)	25 (80.6)	.496
	Yes	20 (30.8)	13 (31)		8 (28.6)	7 (36.8)		5(27.8)	6 (19.4)	
Vascular stenosis	Mild	19 (29.2)	30 (71.4)	< .01*	8 (28.6)	14 (73.7)	.002*	4 (22.2)	20(64.5)	.004*
	Severe	46 (70.8)	12 (28.6)		20 (71.4)	5 (26.3)		14 (77.8)	11 (35.5)	
Radiomics model score	0.8994 ± 0.9148		− 0.1549 ± 1.293	< .01*	0.9931 ± 1.2369	0.4626 ± 0.8025	< .01*	0.8363 ± 0.8039	0.1049 ± 0.7964	.003*

MIS, myocardial ischemia; *No MIS*, non-myocardial ischemia
*$P < 0.05$

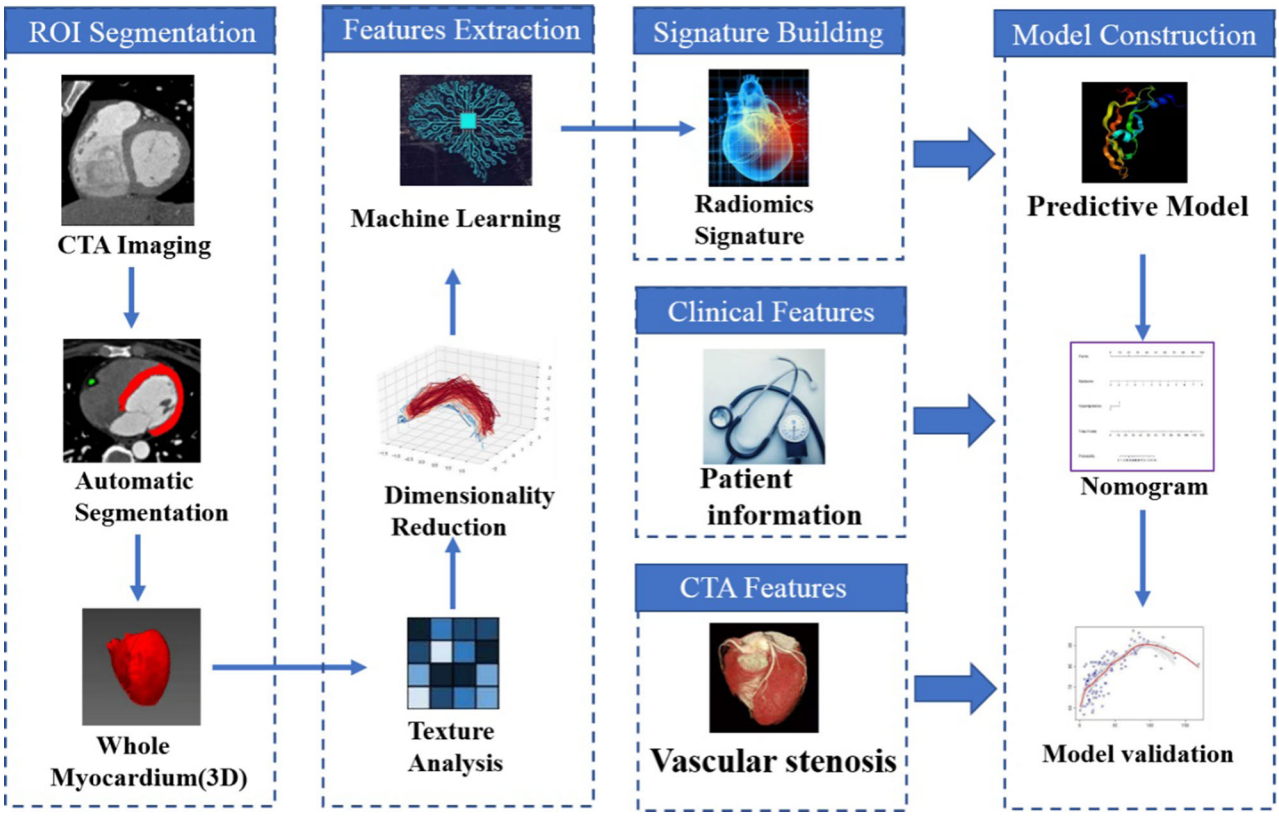

Figure 2. Workflow of the radiomics signature building and model construction.

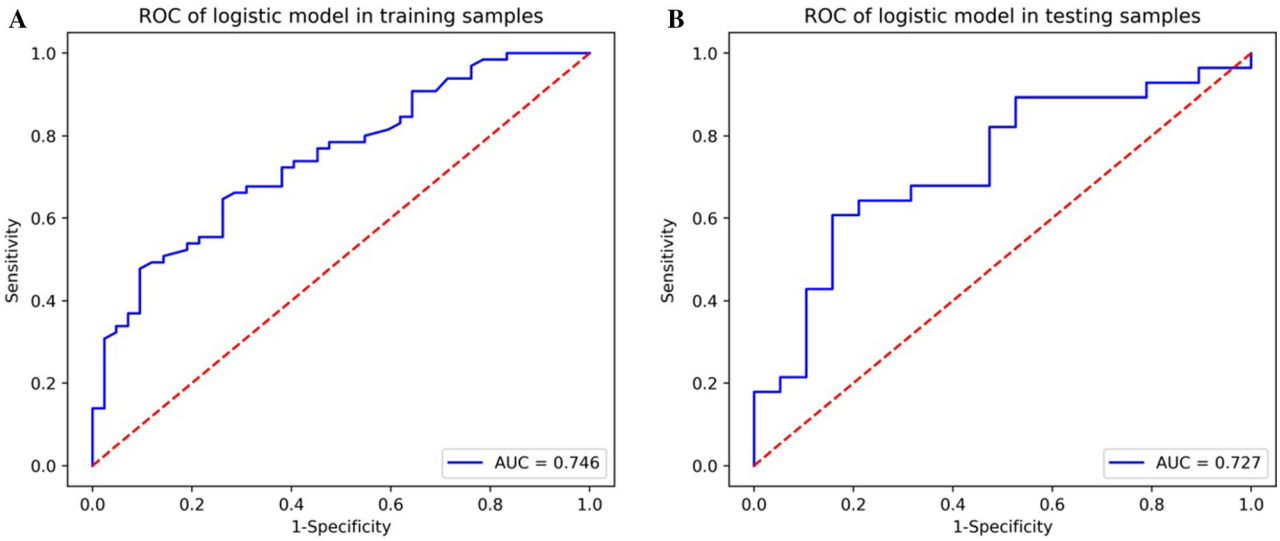

Figure 3. **A** Diagnostic accuracy of the rad-score in the training set and **B** diagnostic accuracy of the rad-score in the test set.

Further, the Hosmer–Lemeshow test showed that there was no statistical difference between the training and test sets ($P > .05$) indicating no deviation from normality.

Performance of Radiomics Nomogram

The accuracy, specificity, and sensitivity of the nomogram for predicting MIS in the training set were 0.839%, 71.4% and 84.6%, respectively. The accuracy, specificity, and sensitivity of the nomogram for predicting MIS in the test set were 0.832%, 68.4% and 82.1%, respectively. The accuracy, specificity, and sensitivity of the nomogram for predicting MIS in the validation set were 0.816%, 70.5%, and 86%, respectively. DCA curves also showed good net benefits in the three sets (Figure 6). Also, we evaluated the accuracy of the radiomics nomogram, radiomics signature and vascular stenosis in all patients using the ROC curve and found AUC to be 0.824, 0.736 and 0.708, respectively. Based on the DeLong test, we found significant differences in AUC between nomogram, vascular stenosis and signature ($P < .0001$, .0026), and no significant difference in AUC between vascular stenosis and label score ($P = .5579$). Nomogram constructed using the training set helped to divide the patients into high-risk and low-risk groups according to the best diagnostic threshold (cut-off value: 0.4388). We observed a significant difference in the number of MIS cases between high-risk and low-risk groups ($P < .001$) (Figure 7).

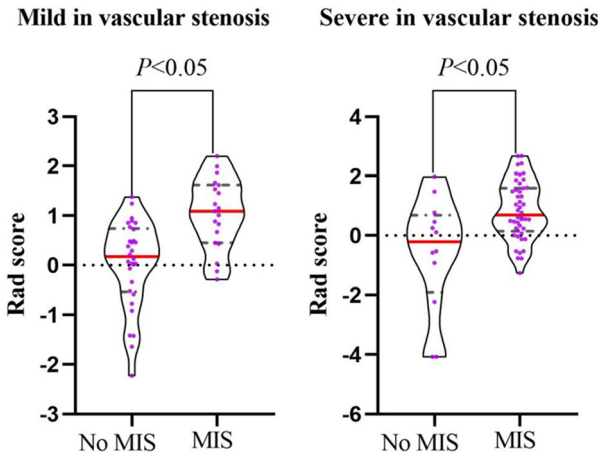

Figure 4. Violin maps of myocardial ischemia predictive score using radiomics signature formula for the mild and severe vascular stenosis subgroups. The red line indicates median and the gray line represents quartile.

DISCUSSION

This proof-of-concept study indicates that radiomics combined with machine learning algorithms help us differentiate non-MIS and MIS in CCTA images. This image analysis extracts information that, in general, may

Table 3. Logistic regression analysis of predicting myocardial ischemia

	Univariate logistic regression		Multivariate logistic regression		
Variable	**OR (95% CI)**	***P* value**	**OR (95% CI)**	***P* value**	**VIF value**
Age (per 1 increase)	0.915 (0.866–0.967)	.002*	NA	NA	
Gender (male vs female)	0.175 (0.041–0.752)	.019*	NA	NA	
Hypertension (no vs yes)	1.2326 (0.315–4.826)	.765	NA	NA	
Diabetes mellitus (no vs yes)	2.391 (0.552–10.357)	.244	NA	NA	
Hyperlipidemia (no vs yes)	1.567 (0.342–7.171)	.563	NA	NA	
Smoking in past 5 years (no vs yes)	0.997 (0.23–4.325)	.996	NA	NA	
Alcohol intake in past 5 years (no vs yes)	0.232 (0.052–1.033)	.055	NA	NA	
Vascular stenosis (non or mild vs severe)	8.709 (6.203–32.878)	< .001*	6.068 (5.762–24.529)	<	0.001*
1.003					
Radiomics score (per 0.1 increase)	4.001 (2.032–7.878)	< .001*	3.817 (1.995–7.306)	<	0.001*
1.024					

NA, not available as the variable was not included in the multivariate logistic regression
*$P < 0.05$

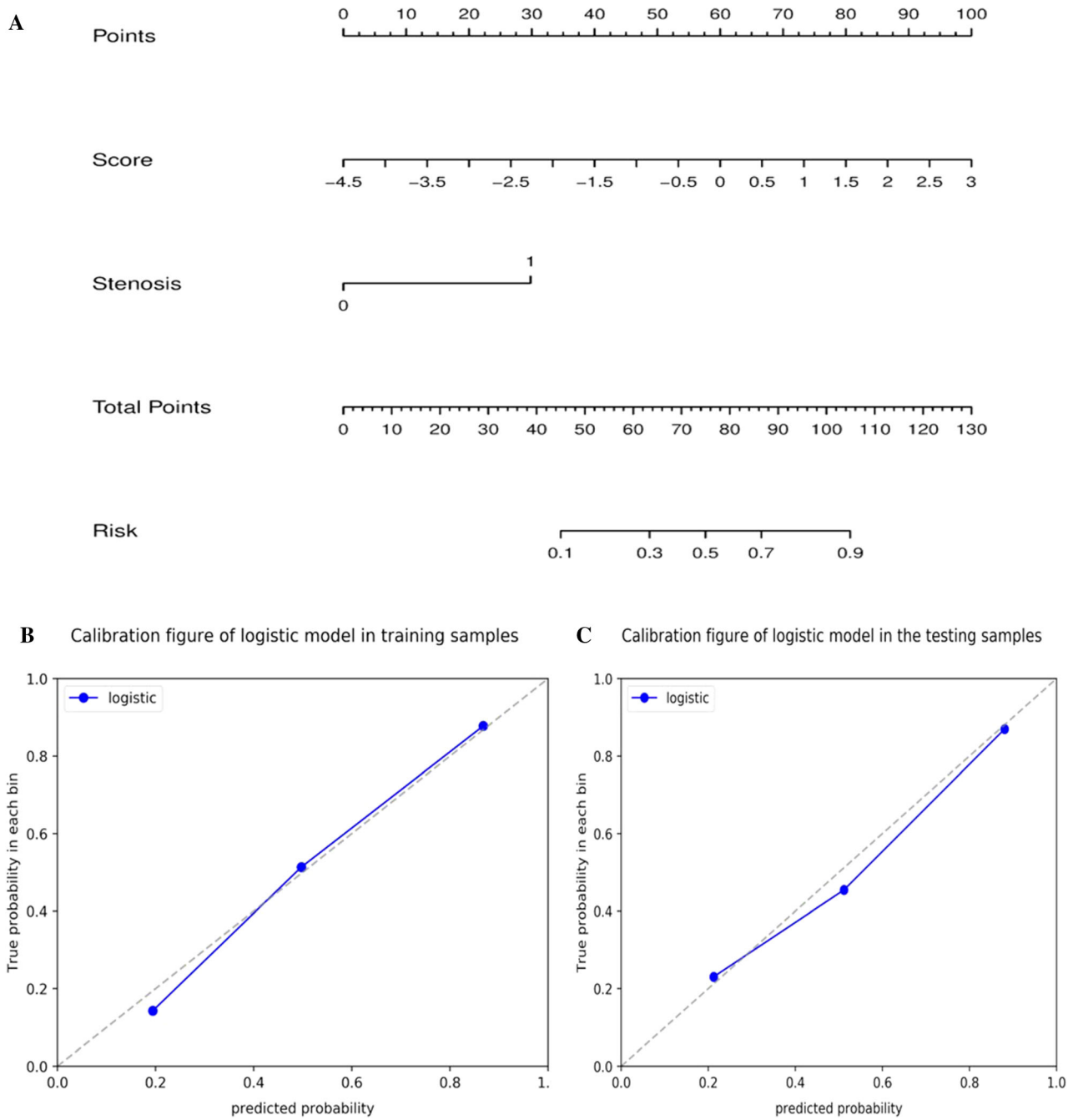

Figure 5. Radiomics nomogram to detect myocardial ischemia (**A**). The radiomics nomogram was developed in the training set with the rad-score and vascular stenosis stage. In the nomogram, we draw a vertical line according to the value of rad-score to determine the corresponding value of points. In the same way, the points of vascular stenosis stage were also determined. Then, total points were the sum of the two points above. Finally, draw a vertical line according to the value of total points to determine the probability of myocardial ischemia. The calibration curve of the radiomics nomogram for myocardial ischemia in the training set (**B**) and test set (**C**). A dashed line indicates the reference line where an ideal nomogram would lie. A dotted line indicates the performance of nomogram, while the solid line indicates bias correction in the nomogram.

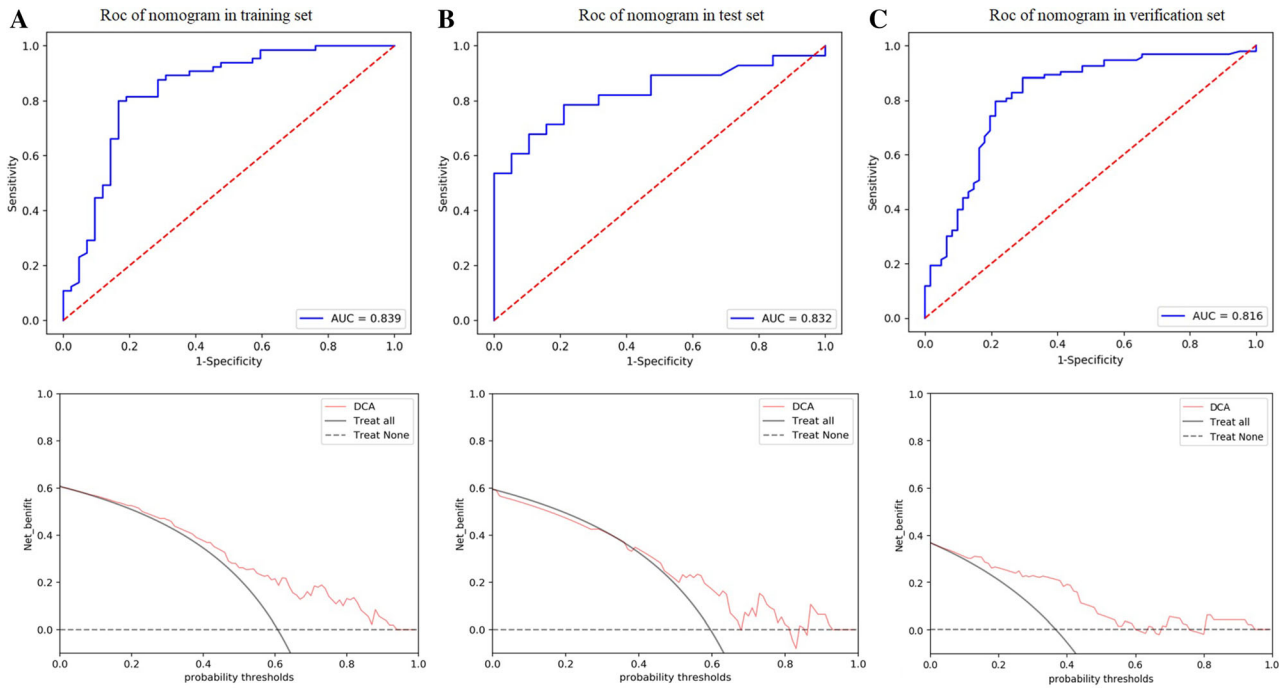

Figure 6. ROC curves of radiomics nomogram to detect the presence of myocardial ischemia in the training, test and validation set, respectively. The decision curve analysis of the training set **A** shows if the threshold probability is between 0 and 0.86. The decision curve analysis of the test set **B** shows if the threshold probability is between 0 and 0.64. The decision curve analysis of the validation set **C** shows if the threshold probability is between 0 and 0.6. Using the radiomics nomogram to predict myocardial ischemia is more beneficial than assuming that all patients suffer from myocardial ischemia or no myocardial ischemia.

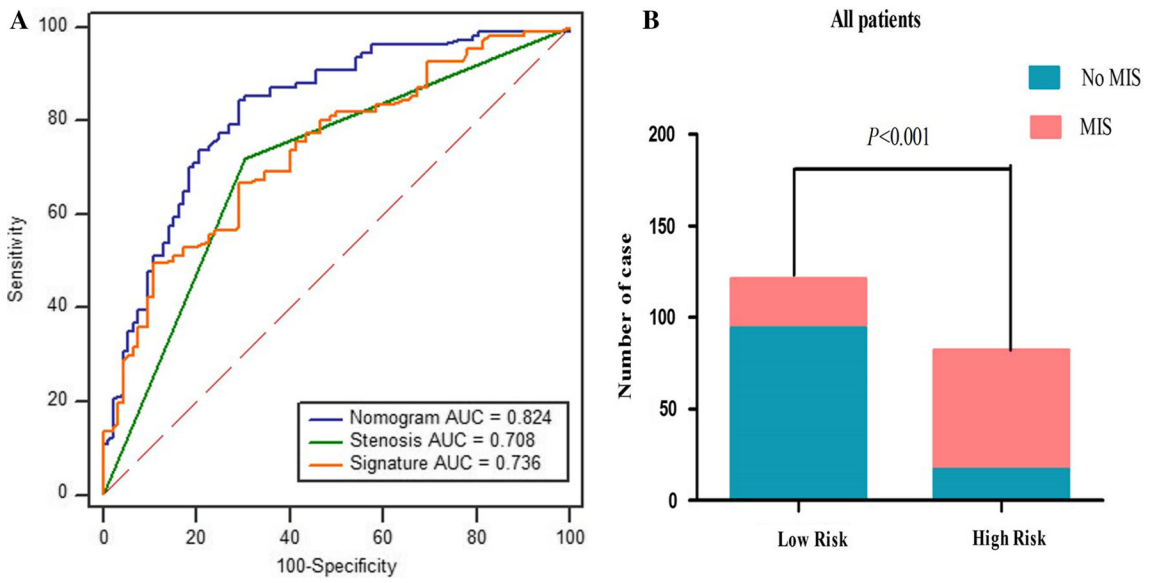

Figure 7. A ROC curves for stenosis, the radiomics signature and nomogram for predicting myocardial ischemia in all 203 patients. **B** The risk classification performance of the nomogram in all 203 patients.

not be visible to the naked eye. Also, the radiomics nomogram incorporating the radiomics signature and CCTA parameters can identify the higher risk population of MIS. This means that it is an accurate and effective tool that predicts MIS in clinical routine. In particular, the radiomics signature of participating in constructing the nomogram also reflects the difference between MIS and non-MIS in the vascular stenosis subgroup, further revealing the prediction mechanism of the nomogram.

CCTA is mainly used in patients with low-to-intermediate cardiovascular risk and it determines the degree of coronary artery stenosis from an anatomical point of view. It is useful in routine follow-up examination of suspected CAD and prediction of high-risk CAD. Also, CCTA is mostly used as the first-line method for the evaluation and prognosis of patients with possible CAD. However, CCTA cannot identify and locate the target blood vessel meaning it cannot provide information on the whole and local MIS directly. This mismatch between results of CCTA and MIS is well known.[35] Hence, CCTA is usually performed in combination with other functional tests to assess MIS.[36] However, in this study, we used radiomics nomogram instead of other functional tests to evaluate MIS. Using SPECT-MPI as a reference standard, the nomogram showed good recognition performance. Although SPECT is the gold standard for diagnosing MIS,[37] we have to realize that SPECT-MPI has a low spatial resolution and it cannot accurately display the anatomical structure of the coronary artery and is highly influenced by artifacts which results in false positives. Thus, SPECT-MPI is not conducive to clinically evaluate early subendocardial ischemia. Also, its application is limited due to the side effects of drugs and excessive exposure to continuous scanning. Therefore, CCTA-based radiomics analysis may be beneficial for patients who cannot tolerate loads of heart imaging tests. Furthermore, CCTA evaluates MIS along with stenosis.

Previous studies have confirmed that the evaluation of plaque characteristics improves the predictive value of lesion-specific ischemia in CCTA.[38,39] But the deficiency is that the evaluation is subjective and different observers witness significant differences. Hence, CAD evaluation primarily depends on visual evaluation of vascular stenosis, which is a reliable indicator of clinical risk stratification in CAD patients.[40] Based on the above knowledge, we constructed a radiomics nomogram with vascular stenosis for the first time and found that the diagnostic accuracy of the nomogram was significantly higher than that of a single radiomics signature model. Furthermore, it was noticed that the diagnostic efficiency of the radiomics signature was higher than that of vascular stenosis indicating that the radiomics signature act as a potential biomarker for predicting MIS. However, the radiomics signature does not provide evidence for a direct assessment of MIS when compared with fractional flow reserve (FFR). It is encouraging to know that the score of the radiomics signature showed a significant difference between MIS and non-MIS in the mild or no visible vascular stenosis subgroup indicating that the mathematical objectivity of radiomics allows the use of conventional CCTA to accurately assess MI rather than using other invasive methods.[41]

The limitation of the contrast resolution of CT leads to the difficulty of recognizing the theoretical density difference between MIS and non-MIS by a vision in conventional CCTA. But, this limitation was resolved by increasing the contrast dose and the radiation dose clinically.[42] However, this increases the risk of radiation dose and causes potential damage to the renal function. Also, improvement in contrast noise not necessarily gets translated into the improvement of visual accuracy, even on delayed enhanced CCTA imaging. On the other hand, radiomics suggest that such changes in visual unavailability can be quickly identified by inexperienced clinicians. This technique is beneficial because it is fast and easy to perform, also does not require additional scanning time, sequences, or contrast agents. It complements the conventional imaging approach and provides a more sensitive marker of the degree of myocardial microstructure disruption/abnormality. It is possible to decode the huge radiomics statistics using ‘‘big data’’ and machine learning easier and also it provides clinically relevant and useable outcomes. In the present study, we found that the high-order radiomics features are robust with respect to the reproducibility. Also, the texture quantifiers are at advanced texture scale, such as the GLCM or RLM, in particular, the demonstrated diagnostic capability, and this is in concurrence with the results of previous studies.[43] It is proved that the microstructural changes in the myocardium can be reflected by high-order radiomics features.[44,45]

All the myocardium were extracted by the automatic segment and it is one of the advantages of this study and based on that radiomics feature analysis was performed. When compared with a manual segment for myocardium, the results of the automatic segment myocardial radiomic analysis are stable as well as it offers a convenient and quick application clinically. To our knowledge, this study is the first radiological analysis of MIS by myocardium through the automatic segment. Previous texture analysis of myocardium is limited to one single slice of CCTA image and when the ischemic area is large this analysis fails to represent the results of all MIS regions. The second major advantage of our study is that MIS analysis was carried out with

radiomics signature that was constructed from a large number of texture features. The diagnostic accuracy of radiomics signature was significantly improved when compared with a single clinical biomarker such as vascular stenosis or Agatston calcium score. Compared with the diagnostic efficacy (AUC:0.84) of predict model with MIS using fractional flow reserve combined with quantitative plaque measurement by Damini et al.[46] the radiomics nomogram not only showed good ability to diagnose MIS but also stratified the high-risk population. CT-based radiomics nomogram is the key non-invasive and easy-to-use tool for clinicians. It accelerates and simplifies the diagnosis process of CAD patients, thus adding more value.

However, this study has some limitations. The study population included patients with different clinical characteristics that lead to selection bias. However, the implementation of exclusion criteria limits the sources of bias. Second, this is a retrospective study; nevertheless, the analysis of this cohort enables the establishment of a preliminary radiomics nomogram and facilitates the future refinement of the nomogram in a larger and more diverse prospective study. Third, this radiomics quantitative CCTA signature to predict ischemia was developed and validated vs. subjective visual assessment of ischemia. Finally, our study population was relatively small. For future studies, we consider using a larger sample size to investigate the potential of radiomics features to differentiate various stages of MIS. Despite these limitations, we are sure that our experience will facilitate CCTA accurate detection of MIS. Our future work will focus on validating the model.

In this study, we showed that by using relatively fast and quantitative tools we can expand the clinical potential feasibility of radiomics nomograms to identify MIS patients. CCTA examination shows the potential advantages of radiological image analysis by objective and quantitative evaluation. Finally, it can help clinicians to make decisions on the diagnosis and treatment of patients undergoing CTA examination.

Disclosures

None.

References

1. Shay CM, Ning H, Daniels SR, et al. Status of cardiovascular health in US adolescents: Prevalence estimates from the National Health and Nutrition Examination Surveys (NHANES) 2005–2010. Circulation 2013;127:1369-76.
2. Montalescot G, Sedltem U, Achenbech S, et al. ESC guidelines on the management of stable coronary artery disease: The task Force on the management of stable coronary artery disease of the European Society of Cardiology. Eur Heart 2013;2013:2949-3003.
3. Patel MR, Dehmer GJ, Hirshfeld JW, et al. ACCF/SCAI/STS/AATS/AHA/ASNC/HFSA/SCCT 2012 Appropriate use criteria for coronary revascularization focused update: a report of the American College of Cardiology Foundation Appropriate Use Criteria Task Force, Society for Cardiovascular Angiography and Interventions, Society of Thoracic Surgeons, American Association for Thoracic Surgery, American Heart Association, American Society of Nuclear Cardiology, and the Society of Cardiovascular Computed Tomography. J Am Coll Cardiol 2012;59:1336.
4. Budoff MJ, Li D, Kazerooni EA, et al. Diagnostic accuracy of noninvasive 64-row computed tomographic coronary angiography (CCTA) compared with myocardial perfusion imaging (MPI): The PICTURE study. A prospective multicenter trial. Acad Radiol 2017;1:22-9.
5. von Ballmoos MW, Haring B, Juillerat P, et al. Metaanalysis: diagnostic performance of low-radiation-dose coronary computed tomography angiography. Ann Intern Med 2011;154:413-20.
6. Hacker M, Jakobs T, Hack N, et al. Sixty-four slice spiral CT angiography does not predict the functional relevance of coronary artery stenoses in patients with stable angina. Eur J Nucl Med Mol Imaging 2007;34:4-10.
7. Meijboom WB, Van Mieghem CA, Van Pelt N, et al. Comprehensive assessment of coronary artery stenoses: Computed tomography coronary angiography versus conventional coronary angiography and correlation with fractional flow reserve in patients with stable angina. J Am Coll Cardiol 2008;52:636-43.
8. Hulten E, Pickett C, Bittencourt MS, et al. Outcomes after coronary computed tomography angiography in the emergency department: a systematic review and meta-analysis of randomized, controlled trials. J Am Coll Cardiol 2013;61:880-92.
9. Ko SM, Song MG, Chee HK, et al. Diagnostic performance of dual-energy CTstress myocardial perfusion imaging: Direct comparison with cardiovascular MRI. Am J Roentgenol 2014;203:605-13.
10. Yoon YE, Choi JH, Kim JH, et al. Noninvasive diagnosis of ischemia-causing coronary stenosis using CT angiography: Diagnostic value of transluminal attenuation gradient and fractional flow reserve computed from coronary CT angiography compared to invasively measured fractional flow reserve. JACC Cardiovasc Imaging 2012;5:1088-96.
11. Mangold S, Gatidis S, Luz O, et al. Single-source dual-energy computed tomography: Use of monoenergetic extrapolation for a reduction of metal artifacts. Invest Radiol 2014;49:788-93.
12. La Grutta L, Toia P, Maffei E, et al. Infarct characterization using CT. Cardiovasc Diagn Ther 2017;7:171-88.
13. Yip SS, Aerts HJ. Applications and limitations of radiomics. Phys Med Biol 2016;61:R150-66.
14. De Albuquerque M, Anjos LG, Maia Tavares de Andrade HM, et al. MRI texture analysis reveals deep gray nuclei damage in amyotrophic lateral sclerosis. J Neuroimaging 2016;26:201-206.
15. Kolossváry M, Kellermayer M, Merkely B, et al. Cardiac computed tomography radiomics: A comprehensive review on radiomic techniques. J Thorac Imaging 2018;33:26-34.
16. Larroza A, Materka A, López-Lereu M, et al. Differentiation between acute and chronic myocardial infarction by means of texture analysis of late gadolinium enhancement and cine cardiac magnetic resonance imaging. Eur J Radiol 2017;92:78-83.
17. Schofield R, Ganeshan B, Kozor R, et al. CMR myocardial texture analysis tracks different etiologies of left ventricular hypertrophy. J Cardiovasc Magn Reson 2016;18:1-2.
18. Baeßler B, Mannil M, Maintz D, et al. Texture analysis and machine learning of non-contrast T1-weighted MR images in

patients with hypertrophic cardiomyopathy-Preliminary results. Eur J Radiol 2018;102:61-7.
19. Baessler B, Luecke C, Lurz J. Cardiac MRI texture analysis of T1 and T2 maps in patients with infarc tlike acute myocarditis. Radiology 2018;289:357-65.
20. Amano Y, Suzuki Y, Yanagisawa F, et al. Relationship between extension or texture features of late gadolinium enhancement and ventricular tachyarrhythmias in hypertrophic cardiomyopathy. Biomed Res Int 2018;2018:4092469.
21. Liang C, Huang Y, He L, et al. The development and validation of a CT-based radiomics signature for the preoperative discrimination of stage I–II and stage III–IV colorectal cancer. Oncotarget 2016;7:31401-12.
22. Huang YQ, Liang CH, He L, et al. Development and validation of a radiomics nomogram for preoperative prediction of lymph node metastasis in colorectal cancer. J Clin Oncol 2016;34:2157-64.
23. Fihn SD, Gardin JM, Abrams J, et al. 2012 ACCF/AHA/ACP/AATS/PCNA/SCAI/STS guideline for the diagnosis and management of patients with stable ischemic heart disease: a report of the American College of Cardiology Foundation/American Heart Association task force on practice guidelines, and the American College of Physicians, American Association for Thoracic Surgery, Preventive Cardiovascular Nurses Association, Society for Cardiovascular Angiography and Interventions, and Society of Thoracic Surgeons. Circulation 2012;126:e354-471.
24. Gensini GG. A more meaningful scoring system for determining the severity of coronary heart disease. Am J Cardiol 1983;51:606.
25. Sun R, Limkin EJ, Vakalopoulou M, et al. A radiomics approach to assess tumour-infiltrating CD8 cells and response to anti-PD-1 or anti-PD-L1 immunotherapy: An imaging biomarker, retrospective multicohort study. Lancet Oncol 2018;19:1180-91.
26. Thawani R, McLane M, Beig N, et al. Radiomics and radiogenomics in lung cancer: A review for the clinician. Lung Cancer 2018;115:34-41.
27. Shu Z, Fang S, Ding Z, et al. MRI-based radiomics nomogram to detect primary rectal cancer with synchronous liver metastases. Sci Rep 2019;9:3374.
28. Wu J, Aguilera T, Shultz D, et al. Early-stage non-small cell lung cancer: Quantitative imaging characteristics of 18F fluorodeoxyglucose PET/CT allow prediction of distant metastasis. Radiology 2016;281:270-8.
29. Mukaka MM. Statistics corner: A guide to appropriate use of correlation coefficient in medical research. Malawi Med J 2012;24:69-71.
30. Unler A, Murat A, Chinnam RB. mr2PSO: A maximum relevance minimum redundancy feature selection method based on swarm intelligence for support vector machine classification. Inf Sci 2011;181:4625-41.
31. Wu Y, Xu L, Yang P, et al. Survival prediction in high-grade osteosarcoma using radiomics of diagnostic computed tomography. EbioMedicine 2018;34:27-34.
32. Parmar C, Grossmann P, Rietveld D, et al. Radiomic machine-learning classifiers for prognostic biomarkers of head and neck cancer. Front Oncol 2015;5:272.
33. O'Brien RM. A caution regarding rules of thumb for variance inflation factors. Qual Quant 2007;41:673-90.
34. Vickers AJ, Van Calster B, Steyerberg EW. Net benefit approaches to the evaluation of prediction models, molecular markers, and diagnostic tests. BMJ 2016;352:i6.
35. Schuijf JD, Wijns W, Jukema JW, et al. Relationship between noninvasive coronary angiography with multi-slice computed tomography and myocardial perfusion imaging. J Am Coll Cardiol 2006;48:2508-14.
36. Ozaki Y, Okumura M, Ismail TF, et al. Coronary CT angiographic characteristics of culprit lesions in acute coronary syndromes not related to plaque rupture as defined by optical coherence tomography and angioscopy. Eur Heart J 2011;32:2814-23.
37. Gaemperli O, Scbepis T, Valenta I, et al. Cardiac image fusion from stand-alone SPECT and CT clinical experience. J Nucl Med 2007;48:696-703.
38. Park HB, Heo R, Hartaigh B, et al. Atherosclerotic plaque characteristics by CT angiography identify coronary lesions that cause ischemia: A direct comparison to fractional flow reserve. JACC Cardiovasc Imaging 2015;8:1-10.
39. Gaur S, Ovrehus KA, Dey D, et al. Coronary plaque quantification and fractional flow reserve by coronary computed tomography angiography identify ischaemia-causing lesions. Eur Heart J 2016;37:1220-7.
40. Nakahara T, Iwabuchi Y, Murakami K. Diagnostic performance of 3D bull's eye display of SPECT and coronary CTA fusion. Cardiovasc Imaging 2016;9:703-11.
41. Leipsic J, Weir-McCall J, Blanke P. FFR_{CT} for complex coronary artery disease treatment planning: new opportunities. Interv Cardiol 2018;13:126-8.
42. Delgado Sánchez-Gracián C, Oca Pernas R, Trinidad López C, et al. Quantitative myocardial perfusion with stress dual-energy CT: Iodine concentration differences between normal and ischemic or necrotic myocardium, initial experience. Eur Radiol 2016;26:3199-207.
43. Antunes S, Esposito A, Palmisanov A, et al. Characterization of normal and scarred myocardium based on texture analysis of cardiac computed tomography images. Conf Proc IEEE Eng Med Biol Soc 2016;2016:4161-4.
44. Mannil M, von Spiczak J, Manka R, et al. Texture analysis and machine learning for detecting myocardial infarction in Noncontrast low-dose computed tomography: Unveiling the invisible. Invest. Radiol 2018;53:338-43.
45. Hinzpeter R, Wagner MW, Wurnig MC, et al. Texture analysis of acute myocardial infarction with CT: First experience study. PLoS ONE 2017;12:e0186876.
46. Damini D, Sara G, Kristian AO, et al. Integrated prediction of lesion-specific ischaemia from quantitative coronary CT angiography using machine learning: A multicentre study. Eur Radiol 2018;28:2655-64.